Three-Phase Optimal Power Flow for Networked Microgrids Based on Semidefinite Programming Convex Relaxation

Yan Huang; Yuntao Ju; Kang Ma; Michael Short; Tao Chen; Ruosi Zhang; Yi Lin

Abstract

Many autonomous microgrids have high penetration of distributed generation (DG) units. Optimal power flow (OPF) is necessary for the optimal dispatch of such networked microgrids (NMGs). Existing convex relaxation methods for three-phase OPF are only applicable to radial networks, not meshed networks. To overcome this limitation, we develop a semidefinite programming (SDP) convex relaxation model, which can be applied to meshed networks and also includes a model of three-phase DG units and on-load voltage regulators with different connection types. The proposed model has higher accuracy than other existing convex relaxation models and the SDP model effectively solves the OPF problem for three-phase meshed networks with satisfactory accuracy, as validated by real 6-bus, 9-bus, and 30-bus NMGs and the IEEE 123-bus test cases. In the SDP model, the convex symmetric-component of the three-phase DG model is shown to be more accurate than three-phase DG that is modelled as three single-phase DG units in three-phase unbalanced OPF. The optimal control variables obtained from the convex relaxation optimization can be used for both the final optimal dispatch strategy and the initial value of non-convex OPF to obtain the globally optimal solution efficiently.

Keywords: networked microgrids; semidefinite programming; optimal power flow; distributed generation; meshed network

1. Introduction

Renewable energy resources for electricity generation, such as solar photovoltaics and wind turbines, are being widely adopted. Energy sources are becoming increasingly geographically dispersed, where traditional centralized power plants are being replaced by distributed generation (DG) units that runs on renewable sources [1]. The presence of DG units brings new characteristics and control complexity to these networks [2]. As renewable generation in the power system increases, microgrids and related technologies are attracting

increasing attention [3]. Networked microgrids (NMGs) interconnect multiple microgrids and provide methods to operate them in the form of clusters. This can improve the reliability of the power supply in distribution networks [4,5].

Optimal power flow (OPF) is necessary for the optimal power dispatch in NMGs [6–8]. The OPF problem is a notoriously difficult non-convex problem due to the large number of non-convex constraints. Reference [9] developed a chordal conversion method based on a convex iteration algorithm to solve the three-phase OPF problem, but the proposed convex iteration algorithm did not guarantee convergence to a globally optimal solution starting with an arbitrary initial point. Convex relaxation methods must be introduced to ensure the convergence of the iteration algorithm and the global optimality of the solution [10]. At present, convex relaxation theory [11,12] is widely used to solve the OPF problem. A relaxed convex problem can be solved relatively easily and reliably [13–15].

There exists three main convex relaxation methods: semidefinite programming (SDP), second-order cone programming (SOCP), and quadratic convex (QC) relaxation. Reference [16] developed an SDP method to solve the OPF problem using a primal-dual interior-point algorithm. In reference [17], sufficient conditions were given to ensure a feasible SDP solution based on the Karush–Kuhn–Tucker (KKT) conditions. Furthermore, reference [18] demonstrated that the SDP method was problematic and inaccurate in some scenarios, and suggested that the convex relaxation process should be improved. Reference [19] developed a method to solve rank-one SDP problems by introducing penalty terms. Reference [20,21] transformed a radial power flow problem into an SOCP formulation, and solved the latter using an SOCP interior-point algorithm. In references [22,23], the characteristics and applications of the SOCP and SDP relaxation methods were compared, and sufficient conditions for accurate relaxations were proposed. However, because of the computation burden caused by the SOCP and SDP, researchers proposed QC methods in polar form. Reference [24] developed a method to reduce the gap between the approximate solution of the QC relaxation and the globally optimal solution. This method could be easily applied to a mixed-integer nonlinear programming formulation to solve for optimal power dispatch due to the increased calculation efficiency over other relaxation methods, and the reduced dual gap. Reference [25] reformulated nonconvex constraints into linear constraints through QC relaxation, providing a tractable relaxed problem.

Existing convex relaxation methods are mainly applied to transmission networks. Some studies focused on radial distribution networks, and fewer still have investigated meshed networks, such as NMGs. References [26,27] developed an SDP convex relaxation model that is applied to OPF for single-phase radial networks. The SDP model demonstrates good performance, but the model is not applicable to meshed networks. Reference

[28] introduced an SOCP convex relaxation model that is applied to OPF for active distribution networks. But the SOCP convex relaxation model is not applicable to meshed networks.

The challenge of convex relaxation methods is to ensure that the relaxed equations are equivalent to the original non-convex constraints. If the relaxation is not accurate, the optimal solution is not useful and cannot be reconciled with the original OPF solution. The rank-one constraint is a necessary condition for tight SDP relaxation. If the relaxed model satisfies the rank-one condition under some assumptions, the SDP relaxation is accurate and the solution is globally optimal to the original problem [29,30]. The SDP relaxation has been proven to be more accurate than SOCP and QC relaxations in most cases [10].

Due to the advantages of the mathematical properties of the SDP convex relaxation method over other relaxation methods, and a lack of previous work on OPF meshed networks, this paper develops an SDP convex relaxation model for three-phase NMGs, incorporating a three-phase DG model and on-load voltage regulators with different connection types. To summarize, this paper makes the following contributions:

1) An SDP convex relaxation model for three-phase NMGs is developed, which can be used to solve the OPF problem for NMGs. The approach achieves global optimality and provides an optimal dispatch strategy for NMGs.

2) Compared with the SDP convex relaxation model in reference [26], the model developed in this paper delivers greater accuracy. The reason for lower accuracy of the existing model in reference [26] is that the proposed semidefinite constraints are not equivalent to those in the original model.

3) Compared with the three-phase DG modelled as three single-phase DG units in reference [31], the symmetric-component-based DG model applied in our method delivers better performance in three-phase unbalanced OPF.

4) Our SDP model is suitable for the three-phase OPF problem for both meshed and radial networks, whereas the existing methods can only be used for radial networks. The case studies presented demonstrate the wide applicability and usability of the proposed model.

The remainder of the paper is organized as follows: Section 2 introduces the SDP convex relaxation model of three-phase microgrids; Section 3 outlines the comparison between the proposed SDP and an existing SDP model; Section 4 introduces the distributed generation SDP model based on symmetric-component method; Section 5 presents case studies and discussions; and conclusions are summarized in Section 6. A flow chart of the paper organization is found in **Fig. 1**.

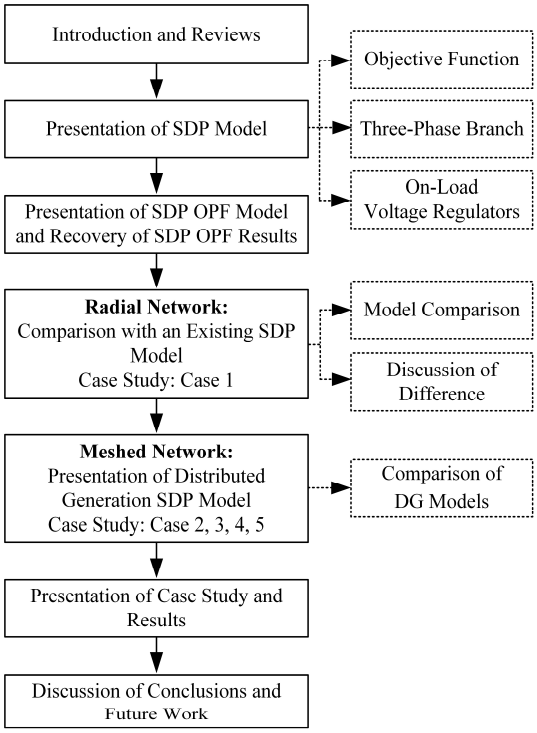

Fig. 1. Flowchart for the paper organization.

2. SDP Convex Relaxation Model

2.1. Objective Function

In this paper, the objective function is to minimize the operation cost of NMGs, as shown below:

$$f = \sum_{i \in G} \left(\sum_{\varphi \in \{a,b,c\}} \left(a_{2i} (P_i^{\varphi})^2 + a_{1i} P_i^{\varphi} + a_{0i} \right) \right) \tag{1}$$

where f indicates the operation cost of the power system; G indicates the set of DG units; P_i^{φ} is the active power on phase φ ($\varphi \in \{A, B, C\}$) of the i_{th} DG unit; a_{2i}, a_{1i}, a_{0i} are the operation cost parameters for the i_{th} DG unit.

The original OPF model has the same objective function as the SDP OPF model. In this paper, P_i^{φ} in Eq. (8) corresponds to P_{iG} in Eq. (13); P_{iG} is a 3×1 matrix.

In the SDP model, the variables are defined as follows.

Voltage variables:

$$V=\left[\dot{U}_1^{abc}\ \dot{U}_2^{abc}\ \cdots\ \dot{U}_N^{abc}\right]\left[\dot{U}_1^{abc}\ \dot{U}_2^{abc}\ \cdots\ \dot{U}_N^{abc}\right]^H \tag{2}$$

where N represents the total number of system buses; V represents the voltage matrix variable of the SDP convex relaxation model, $\dot{U}_1^{abc}=\left[\dot{U}_1^a\ \ \dot{U}_1^b\ \ \dot{U}_1^c\right]^T$, $\dot{U}_2^{abc}=\left[\dot{U}_2^a\ \ \dot{U}_2^b\ \ \dot{U}_2^c\right]^T$, $\dot{U}_N^{abc}=\left[\dot{U}_N^a\ \ \dot{U}_N^b\ \ \dot{U}_N^c\right]^T$ represents the three-phase voltage of 1st bus, 2nd bus and N_{th} bus, respectively; $(.)^H$ denotes the conjugate transpose of $(.)$, and $(.)^T$ denotes the transpose of $(.)$.

Branch power variables:

$$P_f=\left[P_{1f}^a\ \ P_{1f}^b\ \ P_{1f}^c\ \ P_{2f}^a\ \ \cdots\ \ P_{(R-1)f}^c\ \ P_{Rf}^a\ \ P_{Rf}^b\ \ P_{Rf}^c\right] \tag{3}$$

$$Q_f=\left[Q_{1f}^a\ \ Q_{1f}^b\ \ Q_{1f}^c\ \ Q_{2f}^a\ \ \cdots\ \ Q_{(R-1)f}^c\ \ Q_{Rf}^a\ \ Q_{Rf}^b\ \ Q_{Rf}^c\right] \tag{4}$$

$$P_t=\left[P_{1t}^a\ \ P_{1t}^b\ \ P_{1t}^c\ \ P_{2t}^a\ \ \cdots\ \ P_{(R-1)t}^c\ \ P_{Rt}^a\ \ P_{Rt}^b\ \ P_{Rt}^c\right] \tag{5}$$

$$Q_t=\left[Q_{1t}^a\ \ Q_{1t}^b\ \ Q_{1t}^c\ \ Q_{2t}^a\ \ \cdots\ \ Q_{(R-1)t}^c\ \ Q_{Rt}^a\ \ Q_{Rt}^b\ \ Q_{Rt}^c\right] \tag{6}$$

where R indicates the total number of system branches; P_f, Q_f indicates the active power and reactive power injected from the upstream bus of the branch, respectively; P_t, Q_t indicates the active power and reactive power injected to the downstream bus of the branch, respectively; P_{1f}^a indicates, on phase a, the active power injected from the upstream bus of the 1st branch. Here, P_f, Q_f corresponds to p_{ij}, q_{ij} in Eq. (9), respectively; and P_t, Q_t corresponds to $p_{hi}^{'}$, $q_{hi}^{'}$ in Eq. (10), respectively.

DG units power variables:

$$P_g=\left[P_1^a\ \ P_1^b\ \ P_1^c\ \ P_2^a\ \ \cdots\ \ P_{(L-1)}^c\ \ P_L^a\ \ P_L^b\ \ P_L^c\right] \tag{7}$$

$$Q_g=\left[Q_1^a\ \ Q_1^b\ \ Q_1^c\ \ Q_2^a\ \ \cdots\ \ Q_{(L-1)}^c\ \ Q_L^a\ \ Q_L^b\ \ Q_L^c\right] \tag{8}$$

where L indicates the total number of DG units in the system; P_g, Q_g are the matrices of the active and reactive power of DG units, respectively; P_1^a indicates the active power on phase a of the 1st DG units; and Q_1^a indicates the reactive power on phase a of the 1st DG units.

2.2. The SDP Model for Three-Phase Branch

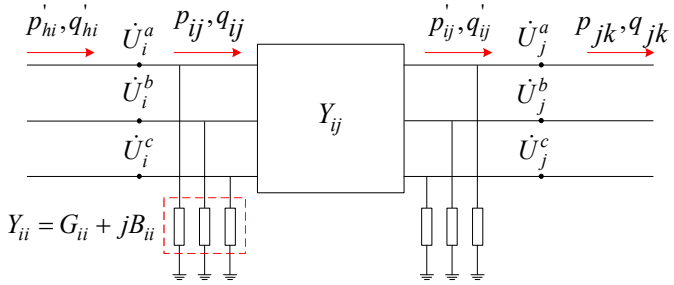

Fig. 2. Three-phase branch diagram.

Fig. 2 presents the three-phase branch diagram. The original three-phase branch power flow constraints are formulated as follows:

$$p_{ij} + \mathrm{j}q_{ij} = \dot{U}_i^{abc} \square \left[(Y_{ij}) \square (\dot{U}_i^{abc} - \dot{U}_j^{abc}) \right]^* \tag{9}$$

$$p'_{hi} + \mathrm{j}q'_{hi} = -\dot{U}_i^{abc} \square \left[(Y_{hi}) \square (\dot{U}_i^{abc} - \dot{U}_h^{abc}) \right]^* \tag{10}$$

$$\underline{S} \le |p_{ij} + \mathrm{j}q_{ij}| \le \overline{S} \tag{11}$$

$$\underline{U} \le |\dot{U}_i^{abc}| \le \overline{U}, \underline{U} \le |\dot{U}_j^{abc}| \le \overline{U} \tag{12}$$

$$\underline{p}_G \le p_{iG} \le \overline{p}_G, \underline{q}_G \le q_{iG} \le \overline{q}_G \tag{13}$$

$$p_{iG} + \sum_{h:h\to i} p'_{hi} = \sum_{j:i\to j} p_{ij} + p_{iD} + \dot{U}_i^{abc} \square (G_{ii} \square \dot{U}_i^{abc})^* \tag{14}$$

$$q_{iG} + \sum_{h:h\to i} q'_{hi} = \sum_{j:i\to j} q_{ij} + q_{iD} + \dot{U}_i^{abc} \square (B_{ii} \square \dot{U}_i^{abc})^* \tag{15}$$

where p_{ij} and q_{ij} are the three-phase branch active and reactive power respectively from the i_{th} bus to j_{th} bus; p_{iG}, p_{iD} indicates the three-phase active power of the i_{th} DG units and the load active power of the i_{th} bus, respectively; q_{iG}, q_{iD} indicates the three-phase reactive power of the i_{th} DG units and the load reactive power of the i_{th} bus, respectively; $\underline{S}$, $\overline{S}$ represents the lower and upper limit of branch complex power, respectively; Y_{ij} indicates the three-phase branch admittance from the i_{th} bus to the j_{th} bus; G_{ii}, B_{ii} represents the shunt conductance and susceptance of the i_{th} bus, respectively; * denotes the complex conjugate; $diag(M)$ means taking the diagonal elements of matrix M to form a vector matrix; $\overline{M}$ and $\underline{M}$ indicate the upper and lower limit of M, respectively; $\square$ denotes matrix operation, $A \square (B)$ represents the one-to-one

multiplication of the elements in the corresponding position of matrix A and matrix B.

Next, the SDP convex relaxation technique is employed to relax Eq. (9). First, Eq. (9) is rewritten as follows:

$$\begin{bmatrix} p_{ij}^{a}+\mathrm{j}q_{ij}^{a} \\ p_{ij}^{b}+\mathrm{j}q_{ij}^{b} \\ p_{ij}^{c}+\mathrm{j}q_{ij}^{c} \end{bmatrix} = \begin{bmatrix} \dot{U}_i^{a} \\ \dot{U}_i^{b} \\ \dot{U}_i^{c} \end{bmatrix} \circ \left(\begin{bmatrix} Y_{ij}^{aa} & Y_{ij}^{ab} & Y_{ij}^{ac} \\ Y_{ij}^{ba} & Y_{ij}^{bb} & Y_{ij}^{bc} \\ Y_{ij}^{ca} & Y_{ij}^{cb} & Y_{ij}^{cc} \end{bmatrix} \circ \left(\begin{bmatrix} \dot{U}_i^{a} \\ \dot{U}_i^{b} \\ \dot{U}_i^{c} \end{bmatrix} - \begin{bmatrix} \dot{U}_j^{a} \\ \dot{U}_j^{b} \\ \dot{U}_j^{c} \end{bmatrix} \right) \right)^{*} \tag{16}$$

Then, Eq. (16) is converted into the following form using the matrix computation theorem [32]:

$$\begin{aligned} \begin{bmatrix} p_{ij}^{a}+\mathrm{j}q_{ij}^{a} \\ p_{ij}^{b}+\mathrm{j}q_{ij}^{b} \\ p_{ij}^{c}+\mathrm{j}q_{ij}^{c} \end{bmatrix} = (Y_{ij})^{*} \circ & \begin{bmatrix} \dot{U}_i^{a} \circ (\dot{U}_i^{a})^{*} & \dot{U}_i^{a} \circ (\dot{U}_i^{b})^{*} & \dot{U}_i^{a} \circ (\dot{U}_i^{c})^{*} \\ \dot{U}_i^{b} \circ (\dot{U}_i^{a})^{*} & \dot{U}_i^{b} \circ (\dot{U}_i^{b})^{*} & \dot{U}_i^{b} \circ (\dot{U}_i^{c})^{*} \\ \dot{U}_i^{c} \circ (\dot{U}_i^{a})^{*} & \dot{U}_i^{c} \circ (\dot{U}_i^{b})^{*} & \dot{U}_i^{c} \circ (\dot{U}_i^{c})^{*} \end{bmatrix}^{T} \\ - (Y_{ij})^{*} \circ & \begin{bmatrix} \dot{U}_i^{a} \circ (\dot{U}_j^{a})^{*} & \dot{U}_i^{a} \circ (\dot{U}_j^{b})^{*} & \dot{U}_i^{a} \circ (\dot{U}_j^{c})^{*} \\ \dot{U}_i^{b} \circ (\dot{U}_j^{a})^{*} & \dot{U}_i^{b} \circ (\dot{U}_j^{b})^{*} & \dot{U}_i^{b} \circ (\dot{U}_j^{c})^{*} \\ \dot{U}_i^{c} \circ (\dot{U}_j^{a})^{*} & \dot{U}_i^{c} \circ (\dot{U}_j^{b})^{*} & \dot{U}_i^{c} \circ (\dot{U}_j^{c})^{*} \end{bmatrix}^{T} \end{aligned} \tag{17}$$

To concisely describe the SDP model, four voltage intermediate variables are defined:

$$v = \begin{pmatrix} \dot{U}_i^{abc} \circ (\dot{U}_i^{abc})^{H} & \dot{U}_i^{abc} \circ (\dot{U}_j^{abc})^{H} \\ \dot{U}_j^{abc} \circ (\dot{U}_i^{abc})^{H} & \dot{U}_j^{abc} \circ (\dot{U}_j^{abc})^{H} \end{pmatrix} = \begin{pmatrix} v_{ii} & v_{ij} \\ v_{ji} & v_{jj} \end{pmatrix} \tag{18}$$

where v_{ii}, v_{ij}, v_{ji} and v_{jj} are the voltage intermediate variables in the SDP model. They are also the submatrices of V in Eq. (2).

Eq. (17) is rewritten as:

$$p_{ij}+\mathrm{j}q_{ij} = (Y_{ij})^{*} \circ (v_{ii})^{T} + (-Y_{ij})^{*} \circ (v_{ij})^{T} \tag{19}$$

Next, the SDP model of three-phase branch-type constraints Eqs. (9)–(15) are derived:

$$\begin{cases} p_{ij}+\mathrm{j}q_{ij} = (Y_{ij})^{*} \circ (v_{ii})^{T} + (-Y_{ij})^{*} \circ (v_{ij})^{T} \\ p_{hi}^{'}+\mathrm{j}q_{hi}^{'} = -(Y_{hi})^{*} \circ (v_{ih})^{T} - (-Y_{hi})^{*} \circ (v_{ii})^{T} \\ \underline{S} \le \ | p_{ij}+\mathrm{j}q_{ij} | \ \le \overline{S} \\ \underline{V} \le diag(V) \le \overline{V} \\ V \ge 0 \\ \underline{p}_G \le p_{iG} \le \overline{p}_G,\ \underline{q}_G \le q_{iG} \le \overline{q}_G \\ p_{iG} + \sum\limits_{h:h\to i} p_{hi}^{'} = \sum\limits_{j:i\to j} p_{ij} + p_{iD} + (G_{ii})^{*} \circ (v_{ii})^{T} \\ q_{iG} + \sum\limits_{h:h\to i} q_{hi}^{'} = \sum\limits_{j:i\to j} q_{ij} + q_{iD} + (B_{ii})^{*} \circ (v_{ii})^{T} \end{cases} \tag{20}$$

where $\overline{V}$, $\underline{V}$ indicates the upper and lower limit of the voltage magnitude in the SDP model, respectively; v_{ih} is the voltage intermediate variable in the SDP model, which is the submatrix of V in Eq. (2).

2.3. On-Load Voltage Regulators Model

For the on-load voltage regulators, Y-Y and Y-Delta are representative connection types, and their SDP models are provided in this section. The SDP models of the Delta-Y and Delta-Delta connections are given in Appendix A. In the OPF model, the transformer ratio is a controllable variable, and it indicates the setting of the voltage regulator tap position under optimal operation [33].

The multiplication of variables will appear in the constraint equations, such as:

$$\dot{U}_i = t\,\dot{U}_j \tag{21}$$

where $\dot{U}_i$, $\dot{U}_j$ represents the voltage on the primary and secondary sides of the voltage regulator, respectively; and t indicates the transformer ratio. According to reference [34], Eq. (21) is relaxed as follows:

$$< t\dot{U}_j >^{\mathrm{M}} \equiv \begin{cases} \dot{U}_i \geq t^l \dot{U}_j + U_j^l t - t^l U_j^l \\ \dot{U}_i \geq t^u \dot{U}_j + U_j^u t - t^u U_j^u \\ \dot{U}_i \leq t^l \dot{U}_j + U_j^u t - t^l U_j^u \\ \dot{U}_i \leq t^u \dot{U}_j + U_j^l t - t^u U_j^l \end{cases} \tag{22}$$

where t^u, t^l indicates the upper and lower limit of variable t, respectively; and U_j^u, U_j^l indicates the upper and lower limit of variable $\dot{U}_j$, respectively.

In this paper, the on-load voltage regulator is equivalent to an impedance in series with an ideal transformer. The three-phase internal impedance of the transformer is referred to the primary side, and the internal impedances all satisfy the branch power flow constraints, as shown in section 2.2. The convex relaxation models of the ideal transformer with different connection types are introduced as follows.

2.3.1. *Y-Y Connection Voltage Regulator SDP Model*

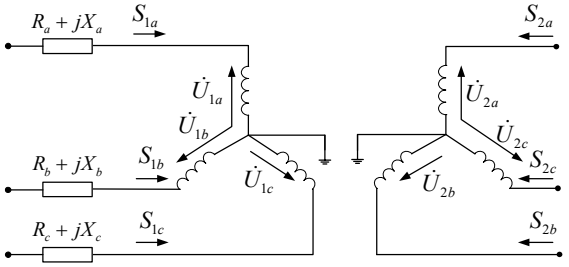

Fig. 3. Y-Y connection type diagram of voltage regulator.

Fig. 3 presents the Y-Y connection type. For the Y-Y connection voltage regulator in the original power flow constraints, the voltage and power relationships between the primary and the secondary sides are given by:

$$\begin{cases} \dot{U}_1^{abc} = T \cdot \dot{U}_2^{abc} \\ S_1 = -S_2 \end{cases} \tag{23}$$

where $\dot{U}_1^{abc} = \begin{bmatrix} \dot{U}_1^a & \dot{U}_1^b & \dot{U}_1^c \end{bmatrix}^T$ and $\dot{U}_2^{abc} = \begin{bmatrix} \dot{U}_2^a & \dot{U}_2^b & \dot{U}_2^c \end{bmatrix}^T$ are the complex voltages of the primary and secondary sides, respectively; S_1 and S_2 are the complex power on the primary and secondary sides, respectively; and T is the three-phase transformer ratio and it is a 3×1 matrix.

Using Eq. (22), Eq. (23) is relaxed as:

$$\begin{cases} u_1 \geq t^l \cdot (u_2) + u_2^l \cdot (t) - t^l \cdot (u_2^l) \\ u_1 \geq t^u \cdot (u_2) + u_2^u \cdot (t) - t^u \cdot (u_2^u) \\ u_1 \leq t^l \cdot (u_2) + u_2^u \cdot (t) - t^l \cdot (u_2^u) \\ u_1 \leq t^u \cdot (u_2) + u_2^l \cdot (t) - t^u \cdot (u_2^l) \\ S_1 = -S_2 \end{cases} \tag{24}$$

where $u_1 = \dot{U}_1^{abc} \cdot (\dot{U}_1^{abc})^H$ and $u_2 = \dot{U}_2^{abc} \cdot (\dot{U}_2^{abc})^H$ are voltage variables in the SDP model; u_2^u, u_2^l indicates the upper and lower limit of variable u_2, respectively; $t = T \cdot (T)^H$ is the transformer ratio.

2.3.2. *Y-Delta Connection Voltage Regulator SDP Model*

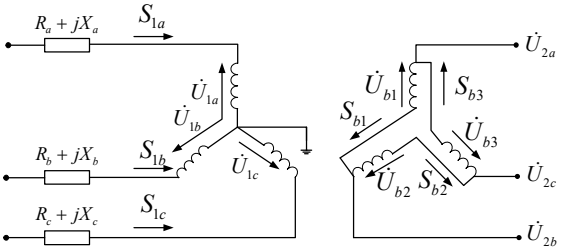

Fig. 4. Y-Delta connection type diagram of voltage regulator.

Fig. 4 presents the Y-Delta connection type. In this case, the voltage and power relationships between the primary and the secondary sides are given by:

$$\begin{cases} \dot{U}_1^{abc} = T \cdot \dot{U}_b \\ \dot{U}_b = B \cdot \dot{U}_2^{abc} \\ S_1 = -S_b \end{cases} \tag{25}$$

where $\dot{U}_b = \begin{bmatrix} \dot{U}_{b1} & \dot{U}_{b2} & \dot{U}_{b3} \end{bmatrix}^T$ represents the secondary line voltage; $B = \begin{bmatrix} -1 & 1 & 0 \\ 0 & -1 & 1 \\ 1 & 0 & -1 \end{bmatrix}$ is the transformation matrix; and $S_b = \begin{bmatrix} S_{b1} & S_{b2} & S_{b3} \end{bmatrix}^T$ represents the secondary branch complex power.

Using Eq. (22), Eq. (25) is relaxed as:

$$\begin{cases} u_1 \geq t^l \cdot (u_b) + u_b^l \cdot (t) - t^l \cdot (u_b^l) \\ u_1 \geq t^u \cdot (u_b) + u_b^u \cdot (t) - t^u \cdot (u_b^u) \\ u_1 \leq t^l \cdot (u_b) + u_b^u \cdot (t) - t^l \cdot (u_b^u) \\ u_1 \leq t^u \cdot (u_b) + u_b^l \cdot (t) - t^u \cdot (u_b^l) \\ u_b = B \cdot u_2 \cdot B^H \\ S_1 = -S_b \end{cases} \tag{26}$$

where $u_b = \dot{U}_b \cdot (\dot{U}_b)^H$ is line voltage in the SDP model; u_b^u, u_b^l indicates the upper and lower limit of variable u_b, respectively.

2.4. Three-Phase SDP OPF Model

To summarize, the variables of the SDP OPF model are defined by: (2), (3), (4), (5), (6), (7) and (8). The

objective function of the SDP OPF is: $\min_{\substack{V,P_g,Q_g,P_f \\ P_t,Q_f,Q_t}}$ (1), subject to: (20) and (24).

2.5. Recover SDP OPF Results

It is important to convert the SDP OPF results into the original OPF results. In the original OPF results, the voltage magnitudes of all buses are given by:

$$\hat{v}_{opt} = \sqrt{diag(\hat{V})} \tag{27}$$

where $\hat{v}_{opt}$ is the voltage magnitudes of all buses in the original OPF model; $\hat{V}$ is the globally optimal voltage solution in the SDP model; $diag(\hat{V})$ means taking the diagonal elements of matrix $\hat{V}$ to form a vector matrix.

To demonstrate how the bus voltage angles are recovered from the SDP OPF results, the three-phase branch SDP model introduced in section 2.2 is taken as an example.

To do the conversion, firstly, the voltage intermediate variable v_{ji} (given by Eq. (18)) in the SDP model is expanded as follows:

$$v_{ji} = \begin{bmatrix} \dot{U}_j^a \square (\dot{U}_i^a)^* & \dot{U}_j^a \square (\dot{U}_i^b)^* & \dot{U}_j^a \square (\dot{U}_i^c)^* \\ \dot{U}_j^b \square (\dot{U}_i^a)^* & \dot{U}_j^b \square (\dot{U}_i^b)^* & \dot{U}_j^b \square (\dot{U}_i^c)^* \\ \dot{U}_j^c \square (\dot{U}_i^a)^* & \dot{U}_j^c \square (\dot{U}_i^b)^* & \dot{U}_j^c \square (\dot{U}_i^c)^* \end{bmatrix} \tag{28}$$

Secondly, the angle difference between phase φ of the i_{th} bus and phase φ of the j_{th} bus is given by:

$$\Delta\theta_{ij}^{\varphi} = \text{atan}\left(\frac{\text{Im}[\dot{U}_j^{\varphi} \square (\dot{U}_i^{\varphi})^*]}{\text{Re}[\dot{U}_j^{\varphi} \square (\dot{U}_i^{\varphi})^*]}\right) \quad \varphi \in \{a,b,c\} \tag{29}$$

where $\Delta\theta_{ij}^{\varphi}$ is the angle difference between phase φ of i_{th} bus and phase φ of j_{th} bus; $\text{Re}[\dot{U}_j^{\varphi} \square (\dot{U}_i^{\varphi})^*]$, $\text{Im}[\dot{U}_j^{\varphi} \square (\dot{U}_i^{\varphi})^*]$ represents the real and imaginary parts of $[\dot{U}_j^{\varphi} \square (\dot{U}_i^{\varphi})^*]$, respectively. The phase angle difference between the head bus and the end bus of all branches can be obtained by applying Eq. (29).

The phase angle of the j_{th} bus is given by:

$$\theta_j^{\varphi} = \theta_i^{\varphi} + \Delta\theta_{ij}^{\varphi} \quad \varphi \in \{a,b,c\} \tag{30}$$

As the voltage angle of the slack bus is defined, the voltage angle of all other buses can be calculated.

3. Comparison with an Existing SDP Model

The SDP model proposed in reference [26] performs well in solving the OPF problem for a radial network, but it cannot be applied to a meshed network. In this section, the model developed in this paper is compared

with the SDP model proposed in reference [26] on a radial network. The numerical results are provided in section 5.1. The radial network case study presented in section 5.1 demonstrates that the SDP model developed in this paper delivers a higher accuracy and better performance when solving the OPF problem for a radial network. In addition, the SDP model was applied to solve the OPF for a meshed network.

3.1. Model Comparison

Take the three-phase branch-type model as an example; the SDP model proposed in reference [26] is shown as follows:

$$\begin{cases} v_{jj} = v_{ii} + Z_{ij}\square i_{ij}\square (Z_{ij})^H - (S_{ij}\square (Z_{ij})^H + Z_{ij}\square (S_{ij})^H) \\ S_j = \sum\limits_{k:j\to k} diag(S_{jk}) - \sum\limits_{i:i\to j} diag(S_{ij} - Z_{ij} i_{ij}) \\ \underline{S} \le S_{ij} \le \overline{S} \\ \underline{S} \le S_{jk} \le \overline{S} \\ \underline{v} \le diag(v_{ii}) \le \overline{v}, \underline{v} \le diag(v_{ij}) \le \overline{v} \\ \begin{pmatrix} v_{ii} & S_{ij} \\ (S_{ij})^H & i_{ij} \end{pmatrix} \ge 0 \end{cases} \tag{31}$$

where $v_{ii} = \dot{U}_i^{abc}\square(\dot{U}_i^{abc})^H$ and $v_{jj} = \dot{U}_j^{abc}\square(\dot{U}_j^{abc})^H$ are voltage intermediate variables in the SDP model; $S_{ij} = \dot{U}_i^{abc}\square(\dot{I}_{ij})^H$ and $S_{jk} = \dot{U}_j^{abc}\square(\dot{I}_{jk})^H$ represent the three-phase branch power from the i_{th} bus to the j_{th} bus and the three-phase branch power from the j_{th} bus to the k_{th} bus, respectively; S_j represents the injection power of j_{th} bus; and Z_{ij} indicates the three-phase branch impedance from the i_{th} bus to the j_{th} bus.

3.2. Discussion of Different SDP Models

In terms of Eqs. (20) and (31), the difference between the two SDP models is mainly in the definition of variables. In the SDP model developed in this paper, the voltage variables Eq. (2) and branch power variables Eqs. (3)–(6) are global variables. For example, for a 30-bus three-phase system, the defined voltage variable is a matrix with a dimension of 90×90. The SDP model proposed in reference [26] defines variables according to the number of branches and buses. These variables are local ones, meaning that the matrix variables are defined for each bus and each branch. For example, for a 30-bus three-phase system, the defined voltage variables are 30 matrices with dimensions of 3×3.

The semidefinite constraints of the two SDP models are different. In this paper, the semidefinite constraint

is presented as follows:

$$V \geq 0 \tag{32}$$

While in reference [26], the semidefinite constraint is presented as:

$$\begin{pmatrix} v_{ii} & S_{ij} \\ (S_{ij})^H & i_{ij} \end{pmatrix} \geq 0 \tag{33}$$

In terms of Eqs. (32) and (33), Eq. (20) includes voltage variables for the entire system, while Eq. (31) is only a semidefinite constraint including local variables of each branch. The two types of semidefinite constraints are not the same and this explains why the two SDP models have different accuracies. The relaxation level of Eq. (32) is tighter and the corresponding SDP OPF is more accurate.

For the radial network, the SDP model has been proven to be accurate for a few classes of optimization problems under a set of assumptions in references [29,30]. If the optimal solution $\widehat{V}$ of the SDP model is a rank-one matrix, then there exists a complex vector $\dot{U}$, which is a globally optimal solution to Eq. (2). For meshed networks, there is currently no strict proof of exactness.

4. Distributed Generation SDP Model

For the OPF problem of NMGs, it is necessary to consider the SDP model of DG units in detail. Storage systems and micro diesel generators can be modeled as a total P and Q controlled bus. Photovoltaic components are currently approximated as fixed generators, whose maximum real and reactive power generation can vary over time [31], which means the total P and Q of photovoltaic components are not controllable due to the intermittency of solar power. The following detailed convex relaxation process is obtained by analyzing the physical characteristics of DG units, and using the symmetric-component method [28,35] to handle the imbalance model.

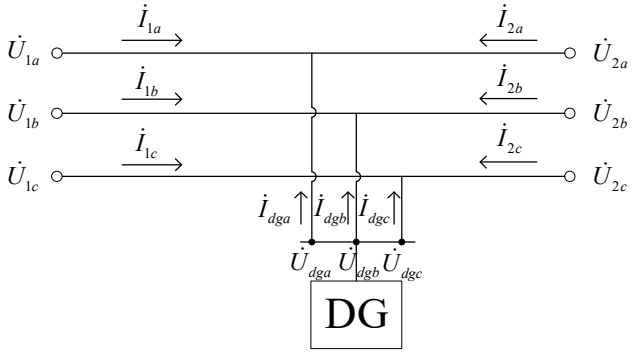

Fig. 5. Typical structure of a DG unit connected to the grid.

Fig. 5 presents the diagram of a DG unit connected to a three-phase network. The DG unit has symmetric structural parameters, and usually uses the symmetric-component model. For a DG unit, the original constraints are as follows:

$$\begin{cases} \dot{U}_{dg}^{seq} = A \cdot \dot{U}_{dg}^{abc} \\ \dot{I}_{dg}^{seq} = A \cdot \dot{I}_{dg}^{abc} \end{cases} \tag{34}$$

where $\dot{U}_{dg}^{seq} = \left[\dot{U}_{dg}^{(0)} \quad \dot{U}_{dg}^{(1)} \quad \dot{U}_{dg}^{(2)} \right]^T$ represents zero-sequence, positive-sequence, and negative-sequence voltage components; $\dot{I}_{dg}^{seq} = \left[\dot{I}_{dg}^{(0)} \quad \dot{I}_{dg}^{(1)} \quad \dot{I}_{dg}^{(2)} \right]^T$ represents zero-sequence, positive-sequence, and negative-sequence current components; $\dot{U}_{dg}^{abc} = \left[\dot{U}_{dg}^{a} \quad \dot{U}_{dg}^{b} \quad \dot{U}_{dg}^{c} \right]^T$ represents the three-phase voltage for DG unit; $\dot{I}_{dg}^{abc} = \left[\dot{I}_{dg}^{a} \quad \dot{I}_{dg}^{b} \quad \dot{I}_{dg}^{c} \right]^T$ represents the three-phase injected current for DG unit; and $A = \frac{1}{3} \begin{bmatrix} 1 & 1 & 1 \\ 1 & \alpha & \alpha^2 \\ 1 & \alpha^2 & \alpha \end{bmatrix}$ is the symmetric-component transformation matrix; $\alpha = e^{j\frac{2}{3}\pi}$.

Here, because the DG units usually use a delta connection transformer to isolate the zero-sequence current, the zero-sequence injected current is zero, as shown below:

$$\begin{cases} \mathrm{Re}(\dot{I}_{dg}^{(0)}) = 0 \\ \mathrm{Im}(\dot{I}_{dg}^{(0)}) = 0 \end{cases} \tag{35}$$

where $\mathrm{Re}(\dot{I}_{dg}^{(0)})$ and $\mathrm{Im}(\dot{I}_{dg}^{(0)})$ represent the real and imaginary parts of the zero-sequence current $\dot{I}_{dg}^{(0)}$, respectively.

If the DG units do not have negative-sequence current control [36], the relationship between the negative-sequence voltage and current conforms to the impedance characteristic and is expressed as an impedance equation, as shown below:

$$\dot{I}_{dg}^{(2)} = \frac{\dot{U}_{dg}^{(2)}}{Z^{(2)}} \tag{36}$$

where $\dot{I}_{dg}^{(2)}$ and $\dot{U}_{dg}^{(2)}$ represent the negative sequence current and negative sequence voltage, respectively, and $Z^{(2)}$ represents the negative impedance.

In this paper, the bus connected to DG unit is equivalent to the total P and Q controlled bus, and the sum of the DG unit three-phase power is constant, as shown below:

$$\begin{cases} S_{total} = \sum\left(S_{dg}\right) \\ S_{dg} = U_{dg}^{abc} \square \left(I_{dg}^{abc}\right)^{*} \end{cases} \tag{37}$$

where S_{dg} represents the three-phase complex power vector of DG, and it is a 3×1 matrix. The notation $\sum(S_{dg})$ indicates the sum of all elements in matrix S_{dg}; S_{total} represents the total injected complex power.

In the SDP model, the variables of DG units are defined as follows:

$$I_{DG} = \begin{bmatrix} \dot{I}_{dg}^{(0)}(\dot{I}_{dg}^{(0)})^{*} & \dot{I}_{dg}^{(0)}(\dot{I}_{dg}^{(1)})^{*} & \dot{I}_{dg}^{(0)}(\dot{I}_{dg}^{(2)})^{*} \\ \dot{I}_{dg}^{(1)}(\dot{I}_{dg}^{(0)})^{*} & \dot{I}_{dg}^{(1)}(\dot{I}_{dg}^{(1)})^{*} & \dot{I}_{dg}^{(1)}(\dot{I}_{dg}^{(2)})^{*} \\ \dot{I}_{dg}^{(2)}(\dot{I}_{dg}^{(0)})^{*} & \dot{I}_{dg}^{(2)}(\dot{I}_{dg}^{(1)})^{*} & \dot{I}_{dg}^{(2)}(\dot{I}_{dg}^{(2)})^{*} \end{bmatrix} \tag{38}$$

$$U_{DG} = \begin{bmatrix} \dot{U}_{dg}^{(0)}(\dot{U}_{dg}^{(0)})^{*} & \dot{U}_{dg}^{(0)}(\dot{U}_{dg}^{(1)})^{*} & \dot{U}_{dg}^{(0)}(\dot{U}_{dg}^{(2)})^{*} \\ \dot{U}_{dg}^{(1)}(\dot{U}_{dg}^{(0)})^{*} & \dot{U}_{dg}^{(1)}(\dot{U}_{dg}^{(1)})^{*} & \dot{U}_{dg}^{(1)}(\dot{U}_{dg}^{(2)})^{*} \\ \dot{U}_{dg}^{(2)}(\dot{U}_{dg}^{(0)})^{*} & \dot{U}_{dg}^{(2)}(\dot{U}_{dg}^{(1)})^{*} & \dot{U}_{dg}^{(2)}(\dot{U}_{dg}^{(2)})^{*} \end{bmatrix} \tag{39}$$

$$S_{DG} = \begin{bmatrix} \dot{U}_{dg}^{(0)}(\dot{I}_{dg}^{(0)})^{*} & \dot{U}_{dg}^{(0)}(\dot{I}_{dg}^{(1)})^{*} & \dot{U}_{dg}^{(0)}(\dot{I}_{dg}^{(2)})^{*} \\ \dot{U}_{dg}^{(1)}(\dot{I}_{dg}^{(0)})^{*} & \dot{U}_{dg}^{(1)}(\dot{I}_{dg}^{(1)})^{*} & \dot{U}_{dg}^{(1)}(\dot{I}_{dg}^{(2)})^{*} \\ \dot{U}_{dg}^{(2)}(\dot{I}_{dg}^{(0)})^{*} & \dot{U}_{dg}^{(2)}(\dot{I}_{dg}^{(1)})^{*} & \dot{U}_{dg}^{(2)}(\dot{I}_{dg}^{(2)})^{*} \end{bmatrix} \tag{40}$$

The notation $I_{DG}[1,1]$ means the 1st row and 1st column of the matrix I_{DG}.

Then, Eqs. (35), (36) and (37) are relaxed as follows:

$$\begin{cases} I_{DG}[1,1] = 0 \\ I_{DG}[3,3] = \dfrac{U_{DG}[3,3]}{Z^{(2)} \square \left[Z^{(2)}\right]^{*}} \\ S_{DG}[1,1] + S_{DG}[2,2] + S_{DG}[3,3] = S_{total} \end{cases} \tag{41}$$

where I_{DG}, U_{DG} and S_{DG} are current, voltage and power variables respectively defined in the above SDP model. Eq. (41) describes the SDP model of DG units.

5. Case Studies

In this section, the SDP model developed in this paper is compared with the SDP model proposed in reference [26], first for a small-scale 6-bus radial network test case and thereafter on the 9-bus, 30-bus, and IEEE 123-bus cases to verify the proposed SDP model. The calculation results of the SDP model are compared with those of the non-convex model to verify the correctness of the SDP model. The system structure and detailed parameters of the test cases were taken from [37]. Here, we use SDPT3 [38] to solve the SDP model and GAMS/SNOPT [39] version 24.7.4 to solve the non-convex model.

To perform error analysis on the SDP model, the maximum absolute error (MAE) and root mean squared error (RMSE) were selected as specifications. The MAE is the maximum absolute error of the bus voltage magnitude between the SDP model and the non-convex model. The RMSE is the standard deviation of the residuals, which are the differences between the values predicted by a model and the values observed [40]. In this paper, the predicted values and the observed values are the results obtained by the SDP model and non-convex model. The combination of these two specifications reasonably demonstrates the calculation accuracy of the SDP model. The two specifications are formulated as follows:

$$\mathrm{MAE} = \max\left\{\left|\,|\dot{U}_i| - |\dot{U}_i^0|\,\right|\right\} \quad i = 1,2,3... \tag{42}$$

$$\mathrm{RMSE} = \sqrt{\frac{1}{N}\sum_{i}^{N}(|\dot{\mathrm{U}}_i| - |\dot{\mathrm{U}}_i^0|)^2} \tag{43}$$

where $|\dot{U}_i|$ represents the voltage magnitude of the i_{th} bus obtained using the SDP model; $|\dot{U}_i^0|$ represents the voltage magnitude of the i_{th} bus obtained using the non-convex model. In this paper, the operation cost parameters of DG units were set to $a_2 = 4$, $a_1 = 1$ and $a_0 = 0$.

5.1. Case 1: 6-Bus Radial Test Case

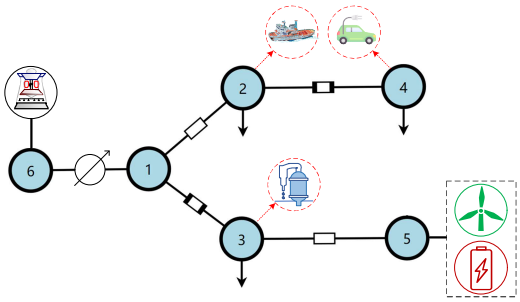

Fig. 6. Diagram of 6-bus three-phase radial network.

Fig. 6 presents a schematic diagram of the 6-bus network. In this case, the objective function is to minimize the operation cost of the DG units connected to bus 5 and bus 6. Please refer to section 2.1 for a detailed description of the mathematical model. Bus 6 is a slack bus, and the rest are PQ buses.

The SDP models developed in this paper and reference [26] are compared with the non-convex model. The results of each bus voltage magnitude and angle are shown below:

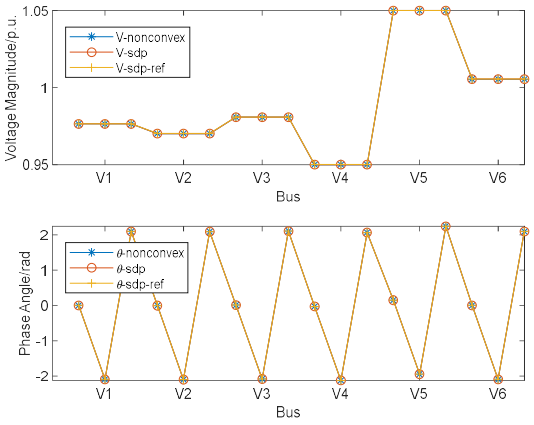

Fig. 7. Comparison of voltage calculation results for 6-bus case.

"V-nonconvex" represents the voltage magnitude calculated using the nonconvex model. "V-sdp" and "V-sdp-ref" represent the voltage magnitudes calculated using the SDP model developed in this paper and in reference [26], respectively. "θ-nonconvex", "θ-sdp", and "θ-sdp-ref" represent the voltage phase angles calculated using the nonconvex model, the SDP model developed in this paper, and the SDP model developed in reference [26], respectively. For the results of the radial network in **Fig. 7**, both SDP models have high accuracy because the voltage magnitudes and phase angles of the two SDP models are approximately consistent with the results of the non-convex model.

Table 1. Comparison of two SDP models calculation results for 6-bus case.

Index	Variable	SDP	SDP-ref
MAE	Voltage magnitude	2.00×10^{-8}	9.02×10^{-5}
	Active power of DG	1.80×10^{-7}	1.67×10^{-6}
	Reactive power of DG	1.13×10^{-6}	1.90×10^{-3}
RMSE	Voltage magnitude	1.34×10^{-8}	7.71×10^{-5}
	Active power of DG	8.05×10^{-8}	7.47×10^{-7}
	Reactive power of DG	6.72×10^{-7}	1.20×10^{-3}

As shown in Table 1, compared with the calculation results from the non-convex model, the MAE and RMSE of the SDP model developed in this paper are smaller, which shows that the model reformulation is more accurate.

5.2. Case 2: 9-Bus Meshed Test Case

In this section, we use a 9-bus multi-phase meshed network case to test the proposed SDP model. **Fig. 8** presents a diagram of the 9-bus meshed network. In this case, the objective function is to minimize the operation cost of the DG units connected to bus 5 and bus 7. Bus 8 and bus 5 are connected by a two-phase line segment and bus 9 and bus 4 are connected by a one-phase line segment.

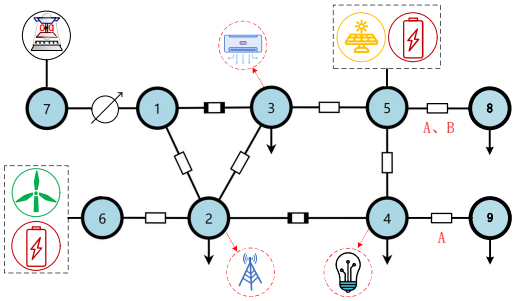

Fig. 8. Diagram of 9-bus multi-phase meshed network structure.

The comparison between the SDP model calculation results and the non-convex model calculation results is as follows:

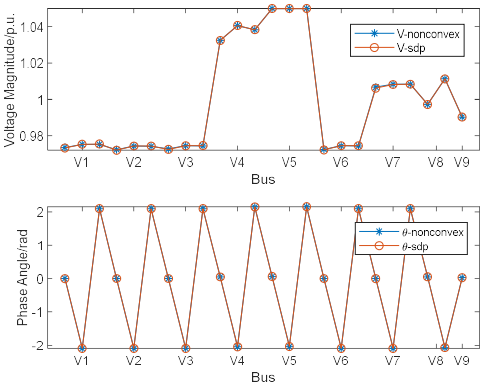

Fig. 9. Comparison of voltage calculation results for 9-bus case.

As shown in **Fig. 9**, the proposed SDP model also performs well in solving the OPF problem of the multi-phase meshed network.

Table 2. Analysis of calculation results for 9-bus meshed case compared with 6-bus radial case.

Index	Variable	SDP for 9-bus meshed network	SDP for 6-bus radial network

MAE	Voltage magnitude	5.10×10^{-4}	2.00×10^{-8}
	Active power of DG	4.10×10^{-3}	1.80×10^{-7}
	Reactive power of DG	6.60×10^{-3}	1.13×10^{-6}
RMSE	Voltage magnitude	1.80×10^{-4}	1.34×10^{-8}
	Active power of DG	1.10×10^{-3}	8.05×10^{-8}
	Reactive power of DG	2.00×10^{-3}	6.72×10^{-7}

Table 2 provides the performance specifications of the SDP model on the 9-bus three-phase meshed network, compared with those of the SDP model on the 6-bus radial network in section 5.1. These indicate that the proposed SDP model is sufficiently accurate to solve the OPF problem for the meshed networks.

5.3. Case 3: 30-Bus Test Case

In this section, we use a larger-scale meshed network to test the proposed SDP model. **Fig. 10** presents a diagram of the 30-bus meshed network. In this case, the objective function is to minimize the operation cost of the DG units connected to bus 5, bus 7, bus 12, and bus 14.

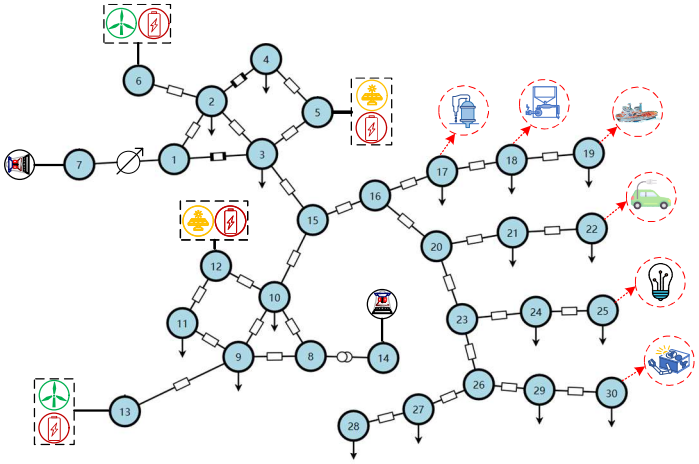

Fig. 10. Diagram of 30-bus three-phase meshed networks structure.

The comparison between SDP model calculation results and non-convex model calculation results is as follows:

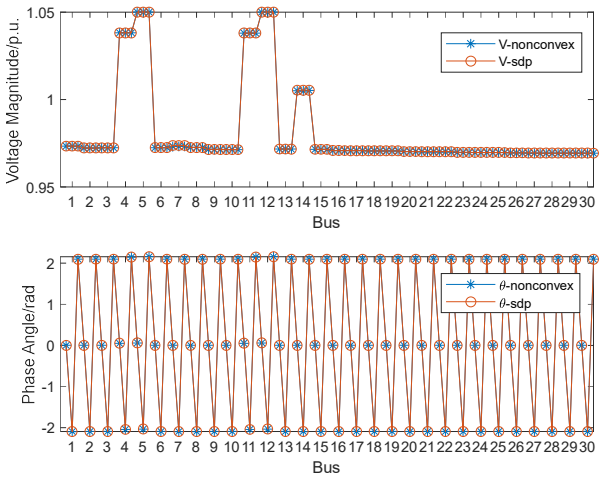

Fig. 11. Comparison of voltage calculation results for 30-bus case.

Table 3. Analysis of SDP model calculation results for 30-bus case.

Indicator	Variable	SDP
MAE	Voltage magnitude	5.96×10^{-4}
	Active power of DG	5.23×10^{-4}
	Reactive power of DG	1.39×10^{-3}
RMSE	Voltage magnitude	1.32×10^{-4}
	Active power of DG	6.59×10^{-5}
	Reactive power of DG	2.90×10^{-4}

It can be concluded from **Fig. 11** and Table 3 that the proposed SDP model is still applicable for large-scale NMGs and performs well.

5.4. Case 4: 123-Bus Test Case

Standard IEEE 123-bus networks including a variety of three-, two-, and one-phase lines were selected for the numerical tests. Only one of the original voltage regulators is considered to be operating using Y-Y connections; others are suppressed. The objective function is to minimize the operation cost of G1 connected to the slack bus.

The comparison between SDP model calculation results and non-convex model calculation results is as follows:

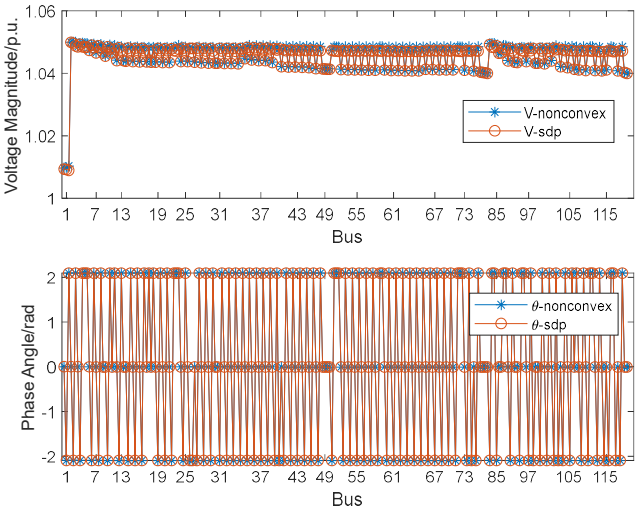

Fig. 12. Comparison of voltage calculation results for IEEE 123-bus case.

Table 4. Analysis of SDP model calculation results for IEEE 123-bus case.

Indicator	Variable	SDP
MAE	Voltage magnitude	1.48×10^{-3}
	Active power of G1	1.94×10^{-6}
	Reactive power of G1	3.38×10^{-6}
RMSE	Voltage magnitude	8.08×10^{-4}
	Active power of G1	1.66×10^{-7}
	Reactive power of G1	2.23×10^{-7}

Fig. 12 and Table 4 present the performance of the SDP model for the IEEE 123-bus multi-phase network. These findings demonstrate that the proposed SDP model is sufficiently accurate to solve the OPF problems on larger-scale networks.

5.5. Case 5: Comparison of Different DG Models

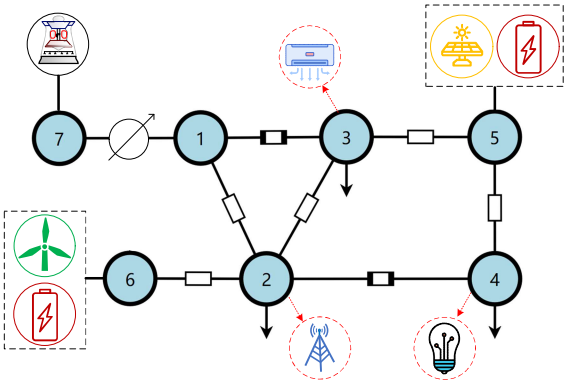

Fig. 13. Diagram of 7-bus three-phase meshed network.

In this section, we analyze the influence of the symmetric-component DG units model and the independent control of the three-phase DG units model [41] on the OPF problem. The three-phase DG units represented with three single-phase DG units do not incorporate the operational constraints between each phase in reference [35]. The numerical test was performed on the 7-bus case using the proposed SDP model under three-phase balance and unbalanced conditions, respectively. **Fig. 13** presents a diagram of the 7-bus meshed network. In this case, the objective function is to minimize the operation cost of the DG units connected to bus 5 and bus 7, and the three-phase constraints of DG units connected to bus 6 is relaxed according to the symmetric-component method introduced in section 4. The numerical results are as follows:

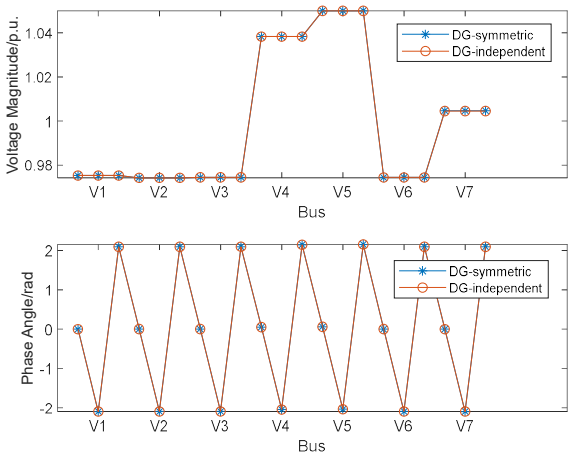

Fig. 14. Comparison of voltage results under three-phase balance.

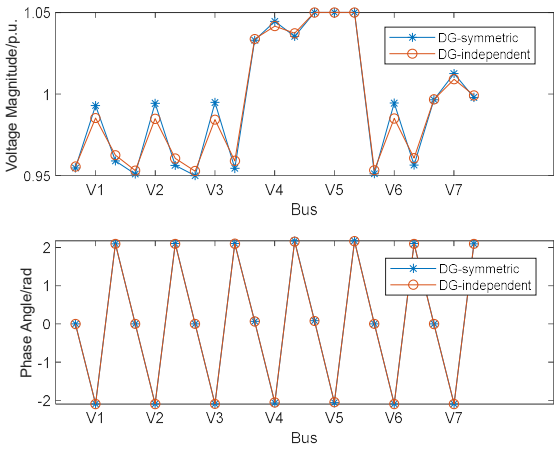

Fig. 15. Comparison of voltage results under three-phase unbalance.

"DG-symmetric" and "DG-independent" represent the symmetric-component DG units model and the three-phase DG model described with three single-phase DG units, respectively. From **Fig. 14** and **Fig. 15**, we can see that using different DG units models has no effect on OPF results under the three-phase balance condition. However, under the three-phase unbalance condition, the OPF results are different. This demonstrates that a three-phase DG units replaced with three-independent single-phase DG units is not accurate for three-phase unbalanced OPF.

6. Conclusions

This paper develops a three-phase semidefinite programming (SDP) relaxation that generalizes the voltage constraints across the entire system, as opposed to merely across individual branches as has been done in previous literature. In the proposed SDP relaxation model, this paper models three-phase distributed generation (DG) units and on-load voltage regulators with different connection types. The proposed SDP relaxation model is a tighter relaxation that is more accurate compared to previous SDP models. The proposed model can be readily extended to three-phase meshed networks, whereas previous models are not applicable to meshed networks. Further, the symmetric-component-based model of DG units used in the proposed method is more accurate than the three-phase DG modeled with three single-phase DG units in existing literature.

The proposed SDP optimal power flow (OPF) model converts the original non-convex problem into a convex problem. It guarantees global optimality of the relaxed model and it also means that the OPF can be solved reliably. The optimal solutions obtained from the proposed SDP model can guide the optimal dispatch of NMGs in real-time. This is important for the safe and optimal operation of the NMGs and it brings economic benefits.

In future research work, energy storage, voltage source converter and other components can be added into the SDP model.

Declaration of Competing Interest

The authors declare that they have no known competing financial interests or personal relationships that could have appeared to influence the work reported in this paper.

Acknowledgments

This research was supported by the National Natural Science Foundation of China (Grant No. 51707196). Calculation resources for this study were provided by the CAU Smart Energy System.

Appendix A

This part mainly considers Delta-Delta and Delta-Y connection types, and their SDP models are given.

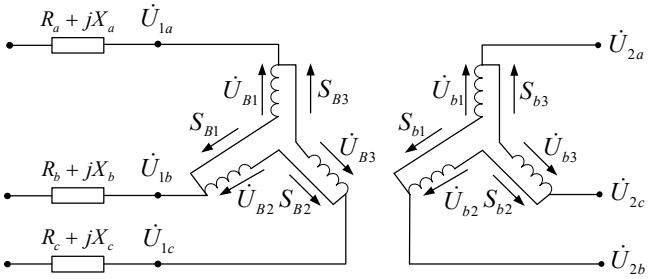

Fig. A1. Delta-Delta connection type diagram of voltage regulator.

Fig. A1 presents the Delta-Delta connection type. In this case, the voltage and power relationships between the primary and the secondary sides are given by:

$$\begin{cases} \dot{U}_B = T \cdot \dot{U}_b \\ \dot{U}_B = B \cdot \dot{U}_1^{abc} \\ \dot{U}_b = B \cdot \dot{U}_2^{abc} \\ S_B = S_b \end{cases} \tag{A1}$$

where $\dot{U}_B = \begin{bmatrix} \dot{U}_{B1} & \dot{U}_{B2} & \dot{U}_{B3} \end{bmatrix}$, $\dot{U}_b = \begin{bmatrix} \dot{U}_{b1} & \dot{U}_{b2} & \dot{U}_{b3} \end{bmatrix}$ represents the primary and secondary line voltage, respectively; $B = \begin{bmatrix} -1 & 1 & 0 \\ 0 & -1 & 1 \\ 1 & 0 & -1 \end{bmatrix}$ is the transformation matrix; and $S_B = \begin{bmatrix} S_{B1} & S_{B2} & S_{B3} \end{bmatrix}$, $S_b = \begin{bmatrix} S_{b1} & S_{b2} & S_{b3} \end{bmatrix}$ represents the primary and secondary branch complex power, respectively.

Using Eq. (22), Eq. (A1) is relaxed as:

$$\begin{cases} u_B \geq t^l \square \left(u_b\right) + u_b^l \square \left(t\right) - t^l \square \left(u_b^l\right) \\ u_B \geq t^u \square \left(u_b\right) + u_b^u \square \left(t\right) - t^u \square \left(u_b^u\right) \\ u_B \leq t^l \square \left(u_b\right) + u_b^u \square \left(t\right) - t^l \square \left(u_b^u\right) \\ u_B \leq t^u \square \left(u_b\right) + u_b^l \square \left(t\right) - t^u \square \left(u_b^l\right) \\ u_B = B \square u_1 \square B^H \\ u_b = B \square u_2 \square B^H \\ S_B = -S_b \end{cases} \tag{A2}$$

where $u_1 = \dot{U}_1^{abc} \square (\dot{U}_1^{abc})^H$ and $u_2 = \dot{U}_2^{abc} \square (\dot{U}_2^{abc})^H$ are voltages in the SDP model; $u_B = \dot{U}_B \square (\dot{U}_B)^H$, $u_b = \dot{U}_b \square (\dot{U}_b)^H$ are line voltages in the SDP model; u_b^u, u_b^l indicates the upper and lower limit of u_b, respectively.

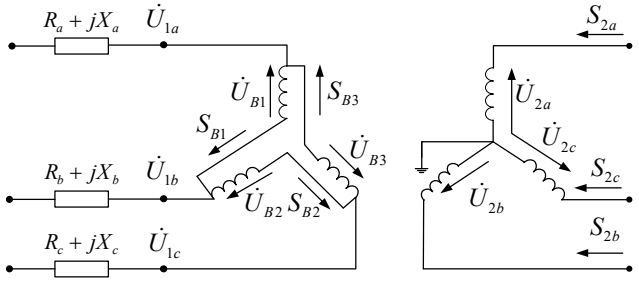

Fig. A2. Delta-Y connection type diagram of voltage regulator.

Fig. A2 presents the Delta-Y connection type. In this case, the voltage and complex power relationships between the primary and the secondary sides are given by:

$$\begin{cases} \dot{U}_B = T \square \dot{U}_2^{abc} \\ \dot{U}_B = B \square \dot{U}_1^{abc} \\ S_B = -S_2 \end{cases} \tag{A3}$$

Using Eq. (22), Eq. (A3) is relaxed as:

$$\begin{cases} u_B \geq t^l \square \left(u_2\right) + u_2^l \square \left(t\right) - t^l \square \left(u_2^l\right) \\ u_B \geq t^u \square \left(u_2\right) + u_2^u \square \left(t\right) - t^u \square \left(u_2^u\right) \\ u_B \leq t^l \square \left(u_2\right) + u_2^u \square \left(t\right) - t^l \square \left(u_2^u\right) \\ u_B \leq t^u \square \left(u_2\right) + u_2^l \square \left(t\right) - t^u \square \left(u_2^l\right) \\ u_B = B \square u_1 \square B^H \\ S_B = -S_2 \end{cases} \tag{A4}$$

References

[1] Ogunmodede O, Anderson K, Cutler D, Newman A. Optimizing design and dispatch of a renewable energy system. Applied Energy 2021;287:116527. https://doi.org/10.1016/j.apenergy.2021.116527.

[2] Kumar RS, Raghav LP, Raju DK, Singh AR. Intelligent demand side management for optimal energy scheduling of grid connected microgrids. Applied Energy 2021;285:116435. https://doi.org/10.1016/j.apenergy.2021.116435.

[3] Xiao H, Pei W, Deng W, Ma T, Zhang S, Kong L. Enhancing risk control ability of distribution network for improved renewable energy integration through flexible DC interconnection. Applied Energy 2021;284:116387. https://doi.org/10.1016/j.apenergy.2020.116387.

[4] Tang C, Liu M, Dai Y, Wang Z, Xie M. Decentralized saddle-point dynamics solution for optimal power flow of distribution systems with multi-microgrids. Applied Energy 2019;252:113361. https://doi.org/10.1016/j.apenergy.2019.113361.

[5] Li J, Liu Y. Optimal Operation for Community-Based Multi-Party Microgrid in Grid-Connected and Islanded Modes. IEEE Transactions on Smart Grid 2018;9:10.

[6] Grover-Silva E, Girard R, Kariniotakis G. Optimal sizing and placement of distribution grid connected battery systems through an SOCP optimal power flow algorithm. Applied Energy 2018;219:385–93. https://doi.org/10.1016/j.apenergy.2017.09.008.

[7] Zhang L, Chen S, Yan Z. Distributed Multi-area Optimal Power Flow Algorithm Based on Blockchain Consensus Mechanism. Proceedings of the CSEE 2020;40:6433–42. https://doi.org/10.13334/j.0258-8013.pcsee.192009.

[8] Carpentier J. Contribution to the economic dispatch problem. Bulletin de La Societe Francoise Des Electriciens 1962;3:431–47.

[9] Wang W, Yu N. Chordal Conversion Based Convex Iteration Algorithm for Three-Phase Optimal Power Flow Problems. IEEE Trans Power Syst 2018;33:1603–13. https://doi.org/10.1109/TPWRS.2017.2735942.

[10] Lin Z, Hu Z, Song Y. Convex Relaxation for Optimal Power Flow Problem: A Recent Review. Proceedings of the CSEE 2019;39:3717–28. https://doi.org/10.13334/j.0258-8013.pcsee.182217.

[11] Boyd S, Vandenberghe L. Convex optimization. Cambridge university press; 2004.

[12] Taylor JA. Convex optimization of power systems. Cambridge University Press; 2015.

[13] Gao H, Liu J, Shen X, Xu B. Optimal power flow research in active distribution network and its application examples. Proceedings of the CSEE 2017;37:1634–45.

[14] Guo Q, Wu J, Mo C. A Model for Multi-objective Coordination Optimization of Voltage and Reactive Power in Distribution Networks Based on Mixed Integer Second-order Cone Programming. Proceedings of the CSEE 2018;38:1385–96.

[15] Shchetinin D, De Rubira TT, Hug G. Efficient Bound Tightening Techniques for Convex Relaxations of AC Optimal Power Flow. IEEE Trans Power Syst 2019;34:3848–57. https://doi.org/10.1109/TPWRS.2019.2905232.

[16] Bai X, Wei H, Fujisawa K, Wang Y. Semidefinite programming for optimal power flow problems. International Journal of Electrical Power & Energy Systems 2008;30:383–92.

[17] Molzahn DK, Lesieutre BC, DeMarco CL. A Sufficient Condition for Global Optimality of Solutions to the Optimal Power Flow Problem. IEEE Trans Power Syst 2014;29:978–9. https://doi.org/10.1109/TPWRS.2013.2288009.
[18] Kocuk B, Dey SS, Sun XA. Inexactness of SDP relaxation and valid inequalities for optimal power flow. IEEE Transactions on Power Systems 2015;31:642–51.
[19] Wu X, Qi H, Xiong N. Rank-one Semidefinite Programming Solutions for Mobile Source Localization in Sensor Networks. IEEE Transactions on Network Science and Engineering 2020;PP:1–1.
[20] Jabr RA. A Conic Quadratic Format for the Load Flow Equations of Meshed Networks. IEEE Trans Power Syst 2007;22:2285–6. https://doi.org/10.1109/TPWRS.2007.907590.
[21] Jabr RA. Radial Distribution Load Flow Using Conic Programming. IEEE Transactions on Power Systems 2006;21:1458–9. https://doi.org/10.1109/TPWRS.2006.879234.
[22] Farivar M, Low SH. Branch Flow Model: Relaxations and Convexification—Part I. IEEE Trans Power Syst 2013;28:2554–64. https://doi.org/10.1109/TPWRS.2013.2255317.
[23] Farivar M, Low SH. Branch Flow Model: Relaxations and Convexification—Part II. IEEE Trans Power Syst 2013;28:2565–72. https://doi.org/10.1109/TPWRS.2013.2255318.
[24] Hijazi H, Coffrin C, Hentenryck PV. Convex quadratic relaxations for mixed-integer nonlinear programs in power systems. Math Prog Comp 2017;9:321–67. https://doi.org/10.1007/s12532-016-0112-z.
[25] Wang X, Bie Z, Liu F, Kou Y. Co-optimization planning of integrated electricity and district heating systems based on improved quadratic convex relaxation. Applied Energy 2021;285:116439. https://doi.org/10.1016/j.apenergy.2021.116439.
[26] Bazrafshan M, Gatsis N, Zhu H. Optimal Power Flow With Step-Voltage Regulators in Multi-Phase Distribution Networks. IEEE Trans Power Syst 2019;34:4228–39. https://doi.org/10.1109/TPWRS.2019.2915795.
[27] Chang C-Y, Zhang W. On exact and near optimal power flow solutions for microgrid applications. 2016 IEEE 55th Conference on Decision and Control (CDC), Las Vegas, NV, USA: IEEE; 2016, p. 4950–6. https://doi.org/10.1109/CDC.2016.7799026.
[28] Ju Y, Huang Y, Zhang R. Optimal Power Flow of Three-Phase Hybrid AC-DC in Active Distribution Network Based on Second Order Cone Programming. Transactions of China Electrotechnical Society 2020;35:51–60. https://doi.org/10.19595/j.cnki.1000-6753.tces.200248.
[29] Low SH. Convex relaxation of optimal power flow—Part I: Formulations and equivalence. IEEE Transactions on Control of Network Systems 2014;1:15–27.
[30] Low SH. Convex relaxation of optimal power flow—Part II: Exactness. IEEE Transactions on Control of Network Systems 2014;1:177–89.
[31] Fobes DM, Claeys S, Geth F, Coffrin C. Power Models Distribution: An open-source framework for exploring distribution power flow formulations. Electric Power Systems Research 2020;189:106664. https://doi.org/10.1016/j.epsr.2020.106664.
[32] A.Hom R, R.Johnson C. Matrix Analysis. Cambridge University Press; 1990.
[33] Acha E, Fuerte-Esquivel CR, Ambriz-Pérez H, Angeles-Camacho C. FACTS: Modelling and Simulation in Power Networks. Chichester, UK: John Wiley & Sons, Ltd; 2004. https://doi.org/10.1002/0470020164.
[34] McCormick GP. Computability of global solutions to factorable nonconvex programs: Part I — Convex underestimating problems. Mathematical Programming 1976;10:147–75. https://doi.org/10.1007/BF01580665.
[35] Kamh MZ, Iravani R. A Unified Three-Phase Power-Flow Analysis Model For Electronically Coupled Distributed Energy Resources. IEEE Trans Power Delivery 2011;26:899–909. https://doi.org/10.1109/TPWRD.2010.2094627.
[36] Gallego LA, Carreno E, Padilha-Feltrin A. Distributed generation modelling for unbalanced three-phase power flow calculations in smart grids. 2010 IEEE/PES Transmission and Distribution Conference and Exposition: Latin America (T&D-LA), Sao Paulo, Brazil: IEEE; 2010, p. 323–8. https://doi.org/10.1109/TDC-LA.2010.5762901.
[37] Huang Y. Microgrid test case feeders 2020. https://github.com/yanhuang-duoduo/Microgrid-test-case.git.

[38] Toh K-C, Todd MJ, Tütüncü RH. SDPT3—a MATLAB software package for semidefinite programming, version 1.3. Optimization Methods and Software 1999;11:545–81.
[39] Gill PE, Murray W, Saunders MA. SNOPT: An SQP Algorithm for Large-Scale Constrained Optimization. SIAM Rev 2005;47:99–131. https://doi.org/10.1137/S0036144504446096.
[40] Mayer MJ, Gróf G. Extensive comparison of physical models for photovoltaic power forecasting. Applied Energy 2021;283:116239. https://doi.org/10.1016/j.apenergy.2020.116239.
[41] Kamh MZ, Iravani R. Steady-State Model and Power-Flow Analysis of Single-Phase Electronically Coupled Distributed Energy Resources. IEEE Trans Power Delivery 2012;27:131–9. https://doi.org/10.1109/TPWRD.2011.2172640.

The English in this document has been checked by at least two professional editors, both native speakers of English. For a certificate, please see:

http://www.textcheck.com/certificate/c4mIjG

The above statement is here to inform reviewers—who may not be native speakers of English—that the English in this document has been professionally checked. If the link to the certificate above is deleted and copied into a letter then the reviewers will not see it.

We STRONGLY recommend that no changes are made. Textcheck should be the last step before final formatting. Typically, authors' changes result in errors in the English, not improvements.

If any text has been misunderstood then please REWRITE the sentence(s) that you need to change, using this file, SAVE, and upload a clean (unmarked) final version of the document

to: http://www.textcheck.com/client/submit for a final check. Please do not mark your changes (no highlighting, colored font, bold, etc.) and do not include notes, questions, or comments. Changes that are not because of misunderstanding may incur additional charges; please see: http://www.textcheck.com/text/page/revisions. Requests for a final check should be made within 1 month. For more detailed information, please see: ‘When you receive your completed document’ at http://www.textcheck.com/text/page/guidelines.

REVISED DOCUMENTS: A previously checked document that needs changed and new sentences checked (such as post review) is termed a ‘Revised Document’ (http://www.textcheck.com/text/page/fees). Revised Documents should be uploaded via 'Submit Document' in your online account, with a note that the file is a revision of '21020918'. Please do not mark your changes; we will use MS Word to compare the document with the most recent complete previous version in your account. When doing so, we cannot consider extracts or versions earlier than the most recent previous version. It is therefore important to upload complete documents. The fee for a Revised Document is based on the wordcount of ALL new and changed sentences. We do not accept new or revised documents on the basis of requests to ‘check only marked text’.